

# Monte-Carlo analysis on registration of $h_c \rightarrow \eta_c + \gamma$ electromagnetic transition in charmonium with PANDA

D. Melnychuk

07.11.2008

## 1. Introduction

According to theoretical predictions and previous experimental observations [1, 7], one of the most promising decay modes for the observation of the  $h_c$  is its electromagnetic transition to the ground charmonium state:

$$h_c \rightarrow \eta_c + \gamma, \quad (1)$$

where the energy of the photon is  $E_\gamma = 503$  MeV. The  $\eta_c$  can be detected through many exclusive decay channels, neutral ( $\eta_c \rightarrow \gamma\gamma$ ) or hadronic. Several selected decay modes of the  $\eta_c$  with the corresponding branching ratios, according to [8], are listed in Table 1.

In order to estimate the signal cross-section we calculate the value of the Breit-Wigner formula at the resonance energy,  $E_R$ :

$$\sigma_p = \frac{3\pi}{k^2} B_{p\bar{p}} B_{\eta_c\gamma}, \quad (2)$$

where  $k^2 = (E_R^2 - 4m_p^2)$  and the  $B$ 's represent the branching ratios into the initial and final states, respectively.

Using the value measured by E835 [1]  $\Gamma_{p\bar{p}} B_{\eta_c\gamma} = 10$  eV and assuming a value of 0.5 MeV for the  $h_c$  width [8] we obtain  $\sigma_p = 33$  nb.

Decay mode	BR
$K_S^0 K^\pm \pi^\mp$	$1.9 \cdot 10^{-2}$
$K_L^0 K^\pm \pi^\mp$	$1.9 \cdot 10^{-2}$
$K^+ K^- \pi^+ \pi^-$	$2.0 \cdot 10^{-2}$
$\pi^+ \pi^- \pi^+ \pi^-$	$1.2 \cdot 10^{-2}$
$K^*(892) \bar{K}^*(892)$	$8.5 \cdot 10^{-3}$
$\phi\phi$	$2.6 \cdot 10^{-3}$
$\gamma\gamma$	$4.3 \cdot 10^{-4}$

Table 1: Decay modes of  $\eta_c$  with the corresponding branching ratios [8]

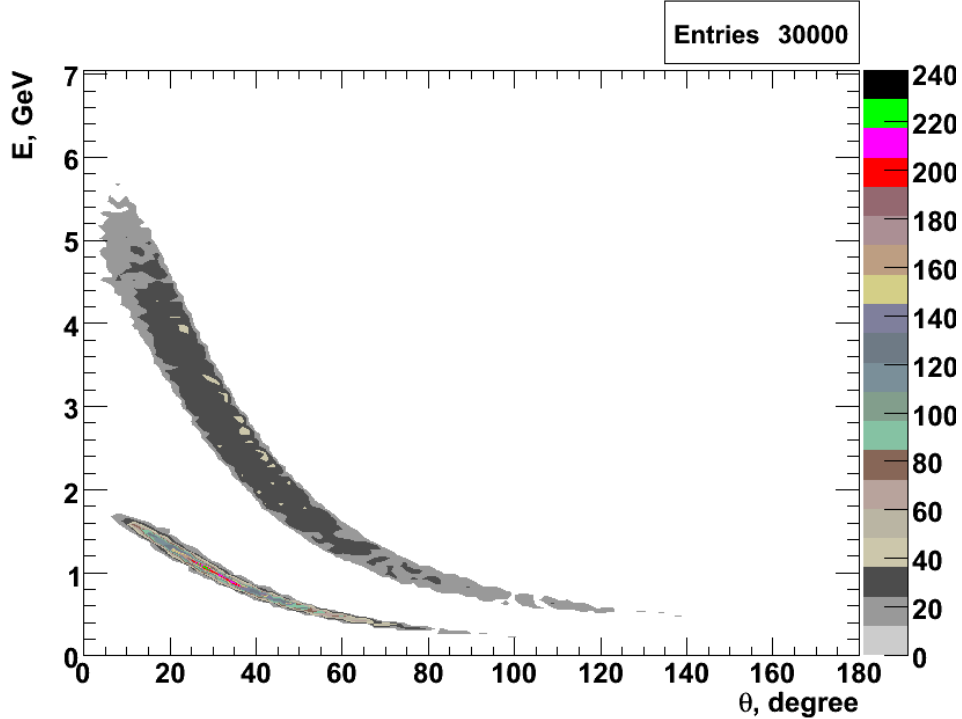


Figure 1: Distribution of events on the  $\gamma$ -ray energy - emission angle plane for the  $h_c \rightarrow \eta_c \gamma \rightarrow 3\gamma$  decay.

## 2. $h_c \rightarrow 3\gamma$ decay mode

This decay mode was observed at Fermilab by E835 [1]. It is characterized by a fairly clean final state, but the low value of the  $\eta_c \rightarrow \gamma\gamma$  branching ratio ( $4.3 \cdot 10^{-4}$ ) (see Table 1) results in a relatively low event rate in comparison with the hadronic decay modes of  $\eta_c$ . The energies of  $\gamma$ 's produced in this decay mode are plotted in Fig. 1 as a function of the polar angle in the laboratory system. The lower band corresponds to  $\gamma$ 's from the radiative transition  $h_c \rightarrow \eta_c \gamma$ . The upper band of highly energetic photons is due to the  $\eta_c \rightarrow \gamma\gamma$  decay. One may note, that an observation of this decay, requires registration of  $\gamma$ 's in the energy range from 150 MeV up to 5.5 GeV.

## Background considerations

The observation of  $h_c$  in  $3\gamma$  final state in proton-antiproton collisions by E835 [1] has demonstrated that it is feasible to achieve sufficient background suppression for this final state, however differences with PANDA in the detector setup require estimation of the degree of background suppression also for the planned experiments. The main contributors to the background for the  $3\gamma$  final state are  $\gamma$ 's from the  $\pi^0$ ,  $\eta$  and  $\eta'$  decay in  $\gamma\gamma$  decay modes: the loss of one or more  $\gamma$ 's outside the detector acceptance or below the energy threshold of the electromagnetic calorimeter (EMC), can result in a  $3\gamma$  final state. The background channels considered in this analysis are listed in Table 2 with the

Channel	Cross-section, nb
$p\bar{p} \rightarrow \pi^0\pi^0$	31.4
$p\bar{p} \rightarrow \pi^0\gamma$	1.4
$p\bar{p} \rightarrow \pi^0\eta$	33.6
$p\bar{p} \rightarrow \eta\eta$	34.0
$p\bar{p} \rightarrow \pi^0\eta'$	50.0

Table 2: The main background contributors to  $h_c \rightarrow 3\gamma$  with the corresponding cross-sections [2, 4] integrated over the range of angles  $|\cos(\theta)| < 0.6$ .

Channel	Number of events
$p\bar{p} \rightarrow h_c \rightarrow 3\gamma$	20 k
$p\bar{p} \rightarrow \pi^0\pi^0$	1.3 M
$p\bar{p} \rightarrow \pi^0\gamma$	100 k
$p\bar{p} \rightarrow \pi^0\eta$	1.3 M
$p\bar{p} \rightarrow \eta\eta$	1.3 M
$p\bar{p} \rightarrow \pi^0\eta'$	100 k

Table 3: Number of generated Monte-Carlo events used in  $h_c \rightarrow 3\gamma$  analysis.

corresponding cross-sections measured by E760 and E835 [1] integrated over the angular range  $|\cos(\theta)| < 0.6$ .

The angular dependence for all the studied background channels is strongly peaked in the forward and backward direction, which is typical for two and three meson production in antiproton-proton annihilations at energies of interest. For the Monte-Carlo study the angular dependence of the cross-sections was parameterized with 6th or 7th order polynomials in  $\cos(\theta)$ . As an example we show in Fig. 2 the angular distribution for the  $\pi^0\gamma$  channel and in Fig. 3 for the channel  $\pi^0\pi^0$ , respectively.

The distribution of events in  $\gamma$ -ray energy emission angle plane for the background channel  $p\bar{p} \rightarrow \pi^0\pi^0$  is shown in Fig. 4. In contrast to the signal (see Fig. 1) events cover the plane starting from zero energy. The forward cut-off in Fig. 4 is caused by event generation over limited range of angles dictated by the experimental data available only in the range  $|\cos(\theta)| < 0.6$ .

## Event selection and background suppression

The number of Monte-Carlo events used for this analysis for signal and all the background channels is collected in Table 3.

The event selection is done in the following steps:

1. An  $\eta_c$  candidate is formed by pairing two  $\gamma$ 's with an invariant mass in the window [2.6; 3.2] GeV. The third  $\gamma$  is added to this pair to form the  $h_c$  candidate.
2. A 4C-fit to beam energy-momentum is applied to the  $h_c$  candidate and the infor-

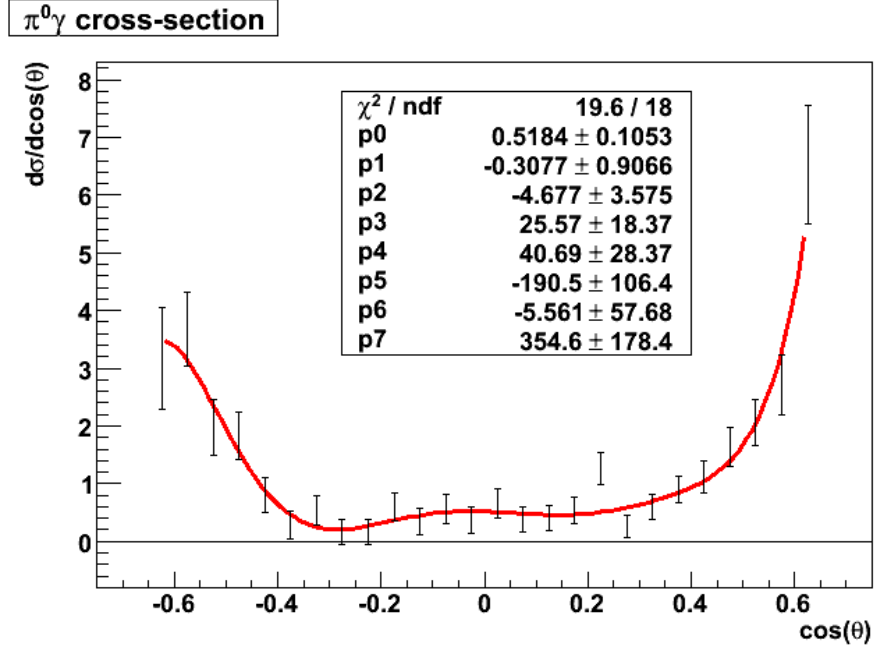


Figure 2: Angular dependence of the  $\pi^0\gamma$  cross-sections parametrized (solid line) with a sum of powers in  $\cos(\theta)$  used in Monte-Carlo simulation. The coefficients of the fit together with their errors are indicated in the inset.

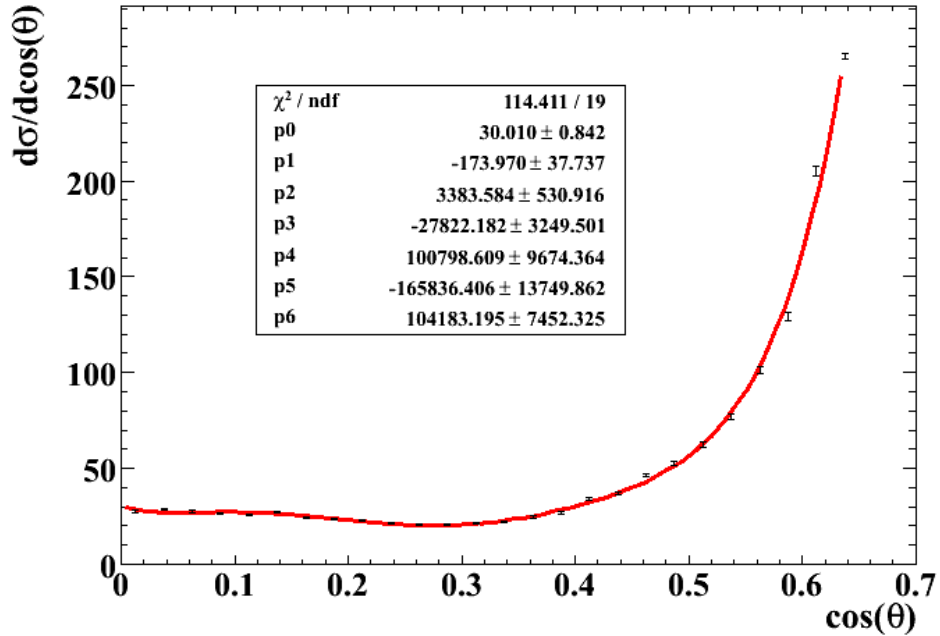


Figure 3: Angular dependence of the  $\pi^0\pi^0$  cross-sections parametrized (solid line) with a sum of powers in  $\cos(\theta)$  used in Monte-Carlo simulation. The coefficients of the fit together with their errors are indicated in the inset.

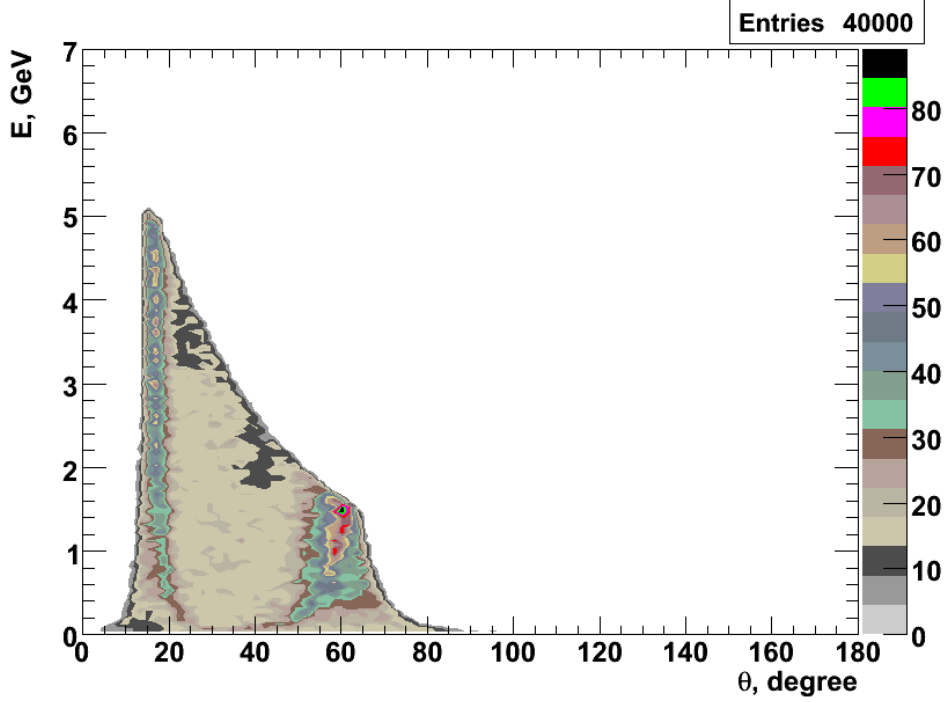


Figure 4: Distribution of events on the energy-emission angle plane for the  $p\bar{p} \rightarrow \pi^0\pi^0$  background channel.

mation on the  $h_c$  and the updated information on the daughter  $\gamma$ 's is stored into the root ntuple.

3. The following cuts are applied at the ntuple level to suppress background:

- (a) Events with  $3\gamma$ 's were selected. This cut keeps 47% of the initial events,
- (b) Cut on the confidence level of the 4C-fit:  $CL > 10^{-4}$ ,
- (c) Cut on the CM energy of the  $\gamma$  from the  $h_c \rightarrow \eta_c\gamma$  radiative transition:  $0.4 \text{ GeV} \leq E_\gamma \leq 0.6 \text{ GeV}$ .
- (d) Angular cut  $|\cos(\theta)| < 0.6$ , to reject the background which is strongly peaked in the forward and backward directions. The  $\cos(\theta)$  distributions for the background channel ( $\pi^0\pi^0$ ) and for the signal are shown in Fig. 14 and Fig. 15, respectively,
- (e) The cut on invariant mass for combinations  $M(\gamma_1, \gamma_3) > 1.0 \text{ GeV}$  and  $M(\gamma_2, \gamma_3) > 1.0 \text{ GeV}$  (the value of the cut is determined by the  $\eta'$  mass).

An impact of the applied selection criteria on the signal and background events is discussed below.

Fig. 5 demonstrates the distribution of  $\gamma$ 's in multiplicity for the signal events; 53% of the events have exactly 3 reconstructed neutral particle candidates. A small fraction of events has less than 3 neutral candidates due to detector acceptance. The events with

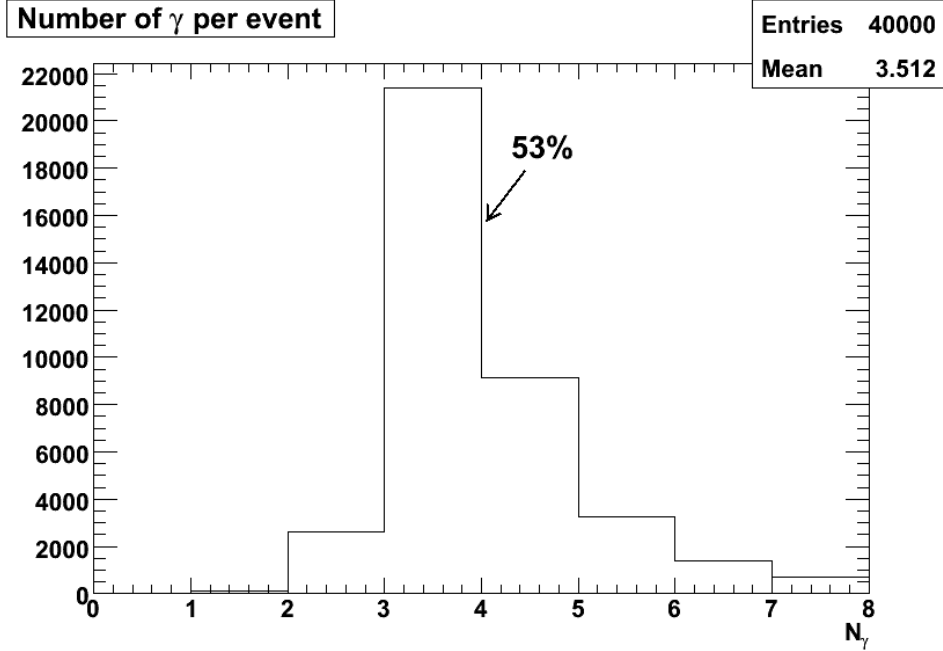


Figure 5: Multiplicity of the reconstructed  $\gamma$ 's in  $h_c \rightarrow \eta_c \gamma \rightarrow 3\gamma$  decay.

$N_\gamma > 3$  are caused by the electromagnetic split-offs. For  $p\bar{p} \rightarrow \pi^0\pi^0$  the distribution of  $\gamma$ 's in multiplicity is shown in Fig. 6; 8% of these events have three neutral candidates. One may conclude, taking into account the ratio of signal to background cross-sections, that the number of background events will exceed the number of expected 3  $\gamma$  events for the signal. A similar situation is encountered for all the remaining background channels listed in Table 2, i.e. they have a significant fraction of 3  $\gamma$  events.

The distribution of confidence level for the 4C-fit to beam energy-momentum for the  $h_c \rightarrow \eta_c \gamma \rightarrow 3\gamma$  events is presented in Fig. 7 in linear and in Fig. 8 in logarithmic scale. The cut is applied at the level  $CL > 10^{-4}$ , as indicated above in the step 3b. Lower values of CL correspond to higher  $\chi^2$  of the fit. The CL distribution is almost flat in the range [0.1; 1.0] for the signal events, whereas for the background channels the probability of higher CL values is lower in general as it can be seen from Fig. 8 for  $p\bar{p} \rightarrow \pi^0\pi^0$  background channel. For many background events the 4C-fit does not converge. Such events get assigned negative CL values and are removed by the  $CL > 10^{-4}$  cut from subsequent analysis.

The  $\gamma$ 's which are combined to  $\eta_c$  are numbered 1 and 2, whereas number 3 is assigned to the  $\gamma$  emitted in the radiative transition  $h_c \rightarrow \eta_c \gamma$ . The distribution of reconstructed energies of the 3<sup>rd</sup>  $\gamma$  in the  $p\bar{p}$  CM system is presented in Fig. 9. The expected energy of the  $\gamma$  emitted in the  $h_c \rightarrow \eta_c \gamma$  transition should be 503 MeV according to the compilation [8]. The reconstructed distribution is peaked close to this value. The range [0.4;0.6] GeV between the two vertical lines defines the limits of the effect (cut 3c). The corresponding distribution for  $\gamma$ 's emitted in  $p\bar{p} \rightarrow \pi^0\pi^0$  is presented in Fig. 10; 40 % of the events for this particular background channel pass the latter selection cut.

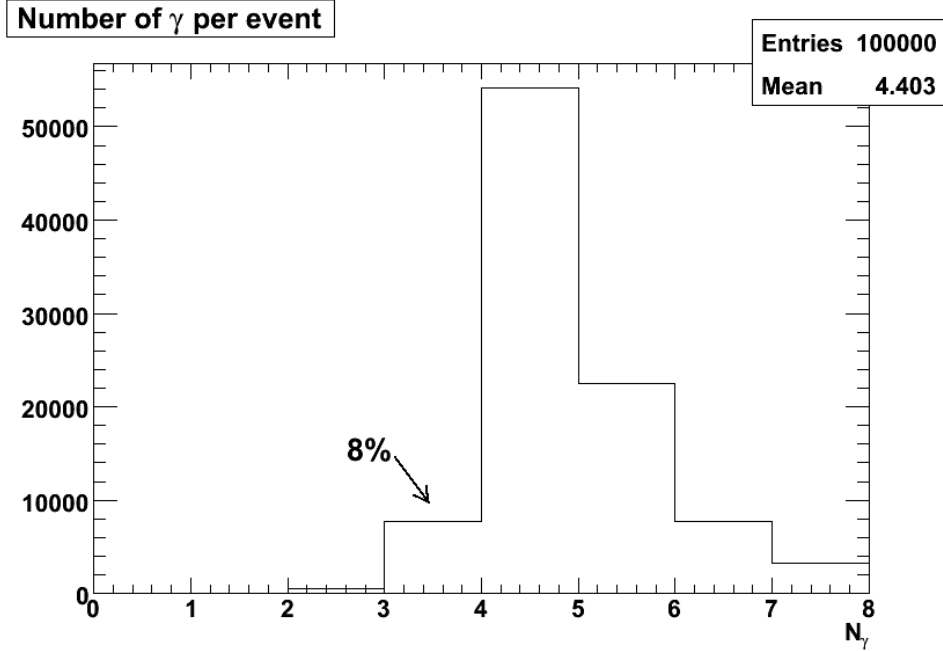


Figure 6: Multiplicity of the reconstructed  $\gamma$ 's in  $p\bar{p} \rightarrow \pi^0\pi^0$  decay.

The distribution of events in the  $E_{\gamma_3}$ -invariant mass  $m(\eta_c)$  plane is presented in Fig. 11 for the  $h_c \rightarrow \eta_c\gamma$  channel. All the events are concentrated along a line which is defined by the applied 4C-fit, consequently, after the fit the  $E_{\gamma_3}$  and  $m(\eta_c)$  variables are no longer independent. The size of boxes is proportional to the number of events in a certain  $E_{\gamma_3}$ ,  $m(\eta_c)$  range. One may note that events are mostly concentrated around the point  $E_{\gamma_3}=0.503$  GeV,  $m(\eta_c)=2.98$  GeV. For the case of  $p\bar{p} \rightarrow \pi^0\pi^0$  background (see Fig. 12) events are more uniformly distributed along the same line.

Fig. 13 presents the reconstructed distribution of the  $\eta_c$  invariant mass. A Breit-Wigner formula, fitted to the simulated data, is superimposed on the figure. The fitted width parameter  $\Gamma = 28$  MeV is slightly larger than the PDG value  $\Gamma_{PDG}=17$  MeV, which illustrates the influence of instrumental resolution,  $\Delta_{exp} \approx 22$  MeV, expected with the PANDA-EMC.

It was mentioned in Sect. 1.1, that the background cross-sections and corresponding intensities of  $\gamma$ 's are peaked in the forward and backward directions. The distribution of the reconstructed  $\gamma_{1,2}$  in  $\cos(\theta)$  in the CM system is shown in Fig. 14 for the  $p\bar{p} \rightarrow \pi^0\pi^0$  channel. An abrupt drop in intensity above  $|\cos(\theta)| > 0.6$  reflects the limits of the generated events, because of the missing experimental information (see the remarks related to Fig. 3). Vertical lines at  $|\cos(\theta)| = 0.6$  indicate the width of the window. In case of the signal (Fig. 15) events have rather flat distribution in  $\cos(\theta)$ , therefore applying a cut eliminating forward and backward angles is a priori expected to improve the signal to background ratio. The two dips are related to the EMC installation: the one at  $\approx 0.35$  reflects irregularity between the barrel and the forward endcap, the other one at  $\approx 0.95$  is an transition between forward endcap and shashlyk calorimeter in Forward Spectrometer.

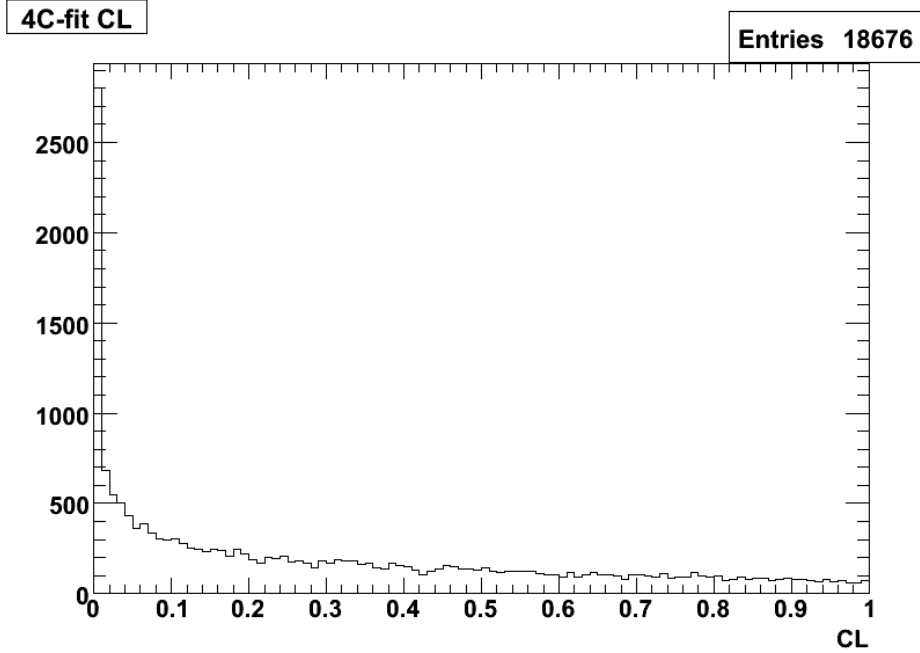


Figure 7: Distribution of confidence level of 4C-fit for  $h_c \rightarrow \eta_c \gamma \rightarrow 3\gamma$ .

Fig. 16 presents the Dalitz plot of  $3\gamma$  events, which pass all the previously mentioned cuts. The signal events are concentrated along the diagonal extending from the top left to the bottom right. Background events from different reactions are marked as red dots. The blue lines mark the selection cuts, i.e.  $M(\gamma_1, \gamma_3) > 1.0\text{GeV}$  and  $M(\gamma_2, \gamma_3) > 1.0\text{GeV}$ . The value of 1 GeV is chosen to eliminate events originating from the  $p\bar{p} \rightarrow \pi^0\eta'$  background channel, i.e. by the mass of  $\eta'$ . None of the background events passes this selection cut and only 37% of the signal events is able to survive, which results in the total signal efficiency of about 8%.

## Summary of the Results

In Table 4 the selection efficiencies for different cuts are presented. Efficiencies are cumulative, i.e. applied one after another. Taking into account the signal cross-section  $\sigma_{p\bar{p} \rightarrow h_c} = 33$  nb at resonance, branching ratio  $BR(\eta_c \rightarrow \gamma\gamma) = 4.3 \cdot 10^{-4}$  and background cross-sections from Table 2 one gets the expected signal to background ratios as listed in Table 5. The expected event rate for running in high luminosity mode,  $L = 2 \cdot 10^{32} \text{cm}^{-2} \text{s}^{-1}$ , is 20 events/day, and for high resolution mode with  $L = 2 \cdot 10^{31} \text{cm}^{-2} \text{s}^{-1}$ , 2.0 events/day, respectively.

### 3. $h_c \rightarrow \gamma\phi\phi$ decay mode

As a benchmark channel with a hadronic decay mode of the  $\eta_c$  we study the  $\phi\phi$  final state with  $BR = 2.6 \cdot 10^{-3}$ . We detect the  $\phi$  through the decay correspondingly  $\phi \rightarrow K^+K^-$ ,

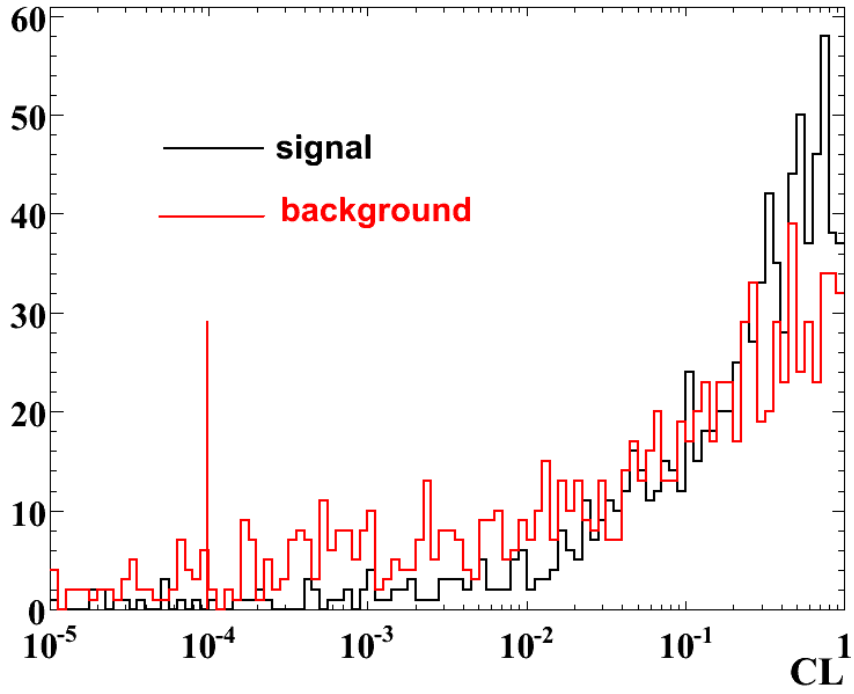


Figure 8: Distribution of confidence level of 4C-fit for  $h_c \rightarrow \eta_c \gamma \rightarrow 3\gamma$  and  $p\bar{p} \rightarrow \pi^0 \pi^0$  background events in logarithmic scale.

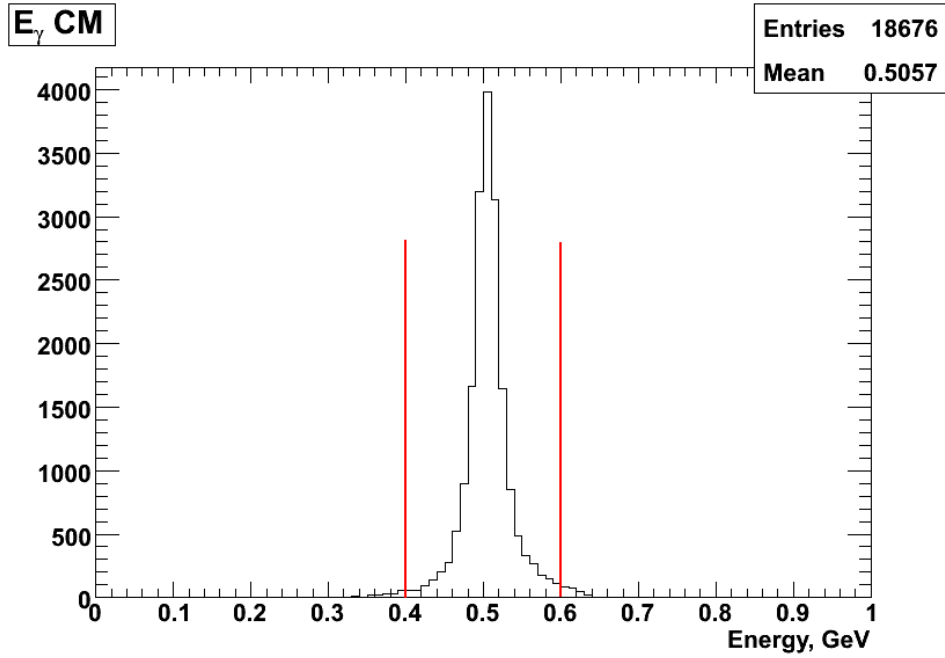


Figure 9: Distribution of reconstructed energy of  $\gamma$  from  $h_c \rightarrow \eta_c \gamma$  radiation transition.

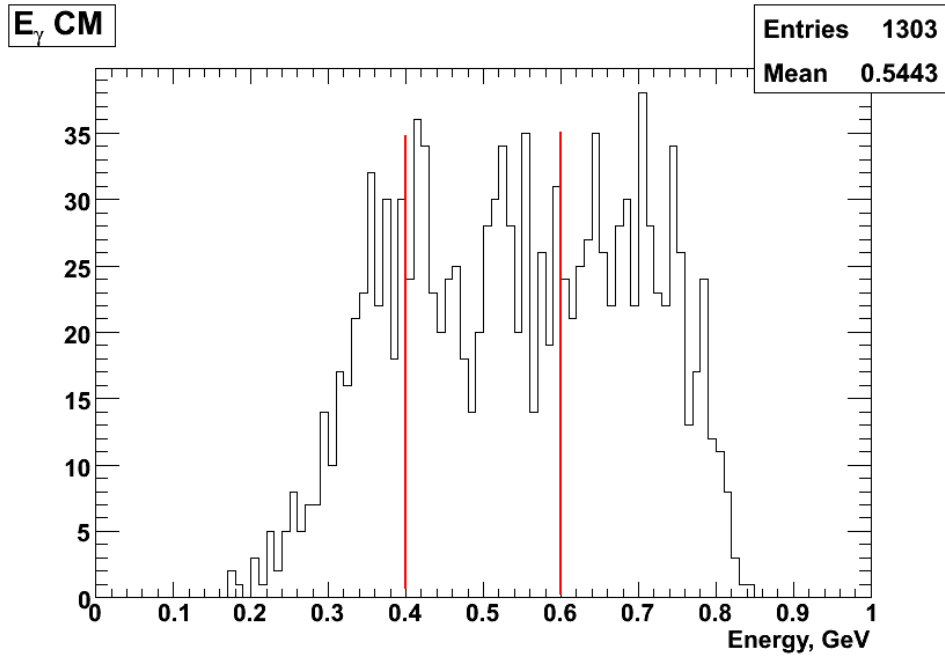


Figure 10: Distribution of reconstructed energy of  $\gamma$  assigned to  $h_c \rightarrow \eta_c \gamma$  radiation transition from  $p\bar{p} \rightarrow \pi^0 \pi^0$  background.

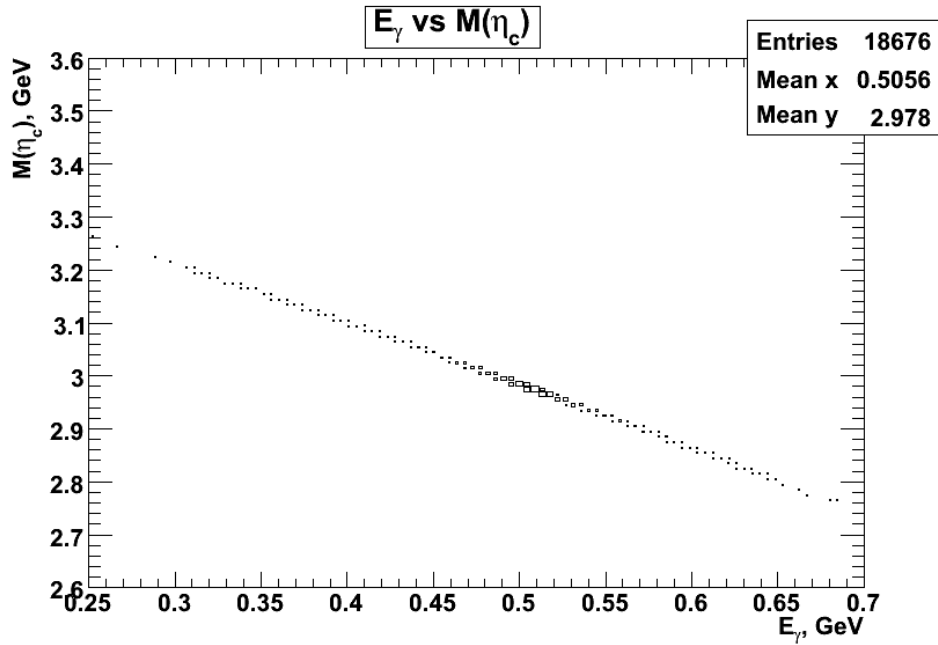


Figure 11: Distribution of reconstructed energy of  $\gamma$  versus  $\eta_c$  invariant mass for  $h_c \rightarrow \eta_c \gamma$ .

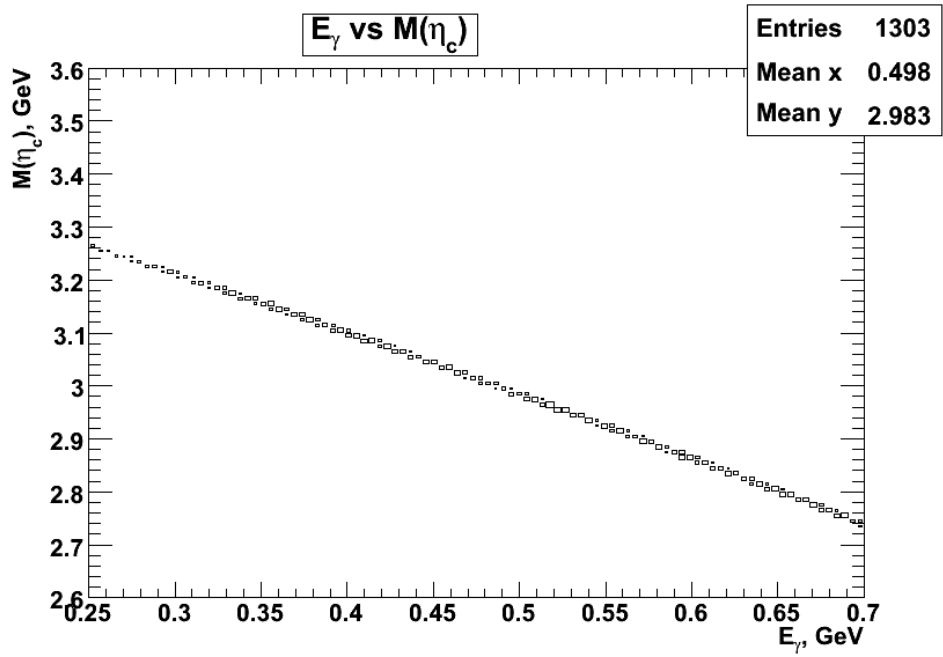


Figure 12: Distribution of reconstructed energy of  $\gamma$  versus  $\eta_c$  invariant mass for  $p\bar{p} \rightarrow \pi^0\pi^0$  background.

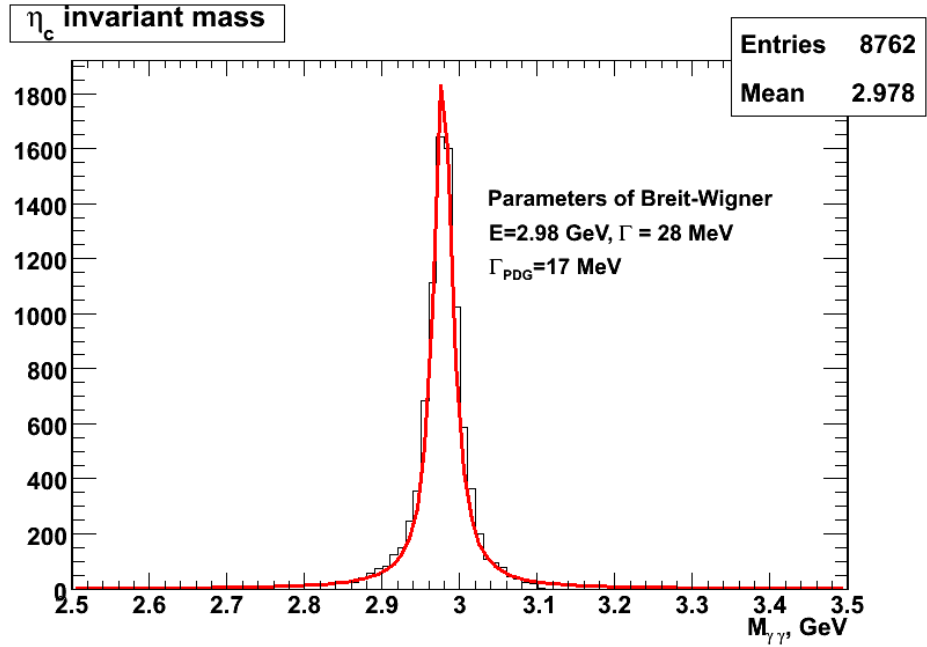


Figure 13: Reconstructed invariant mass of  $\eta_c$ .

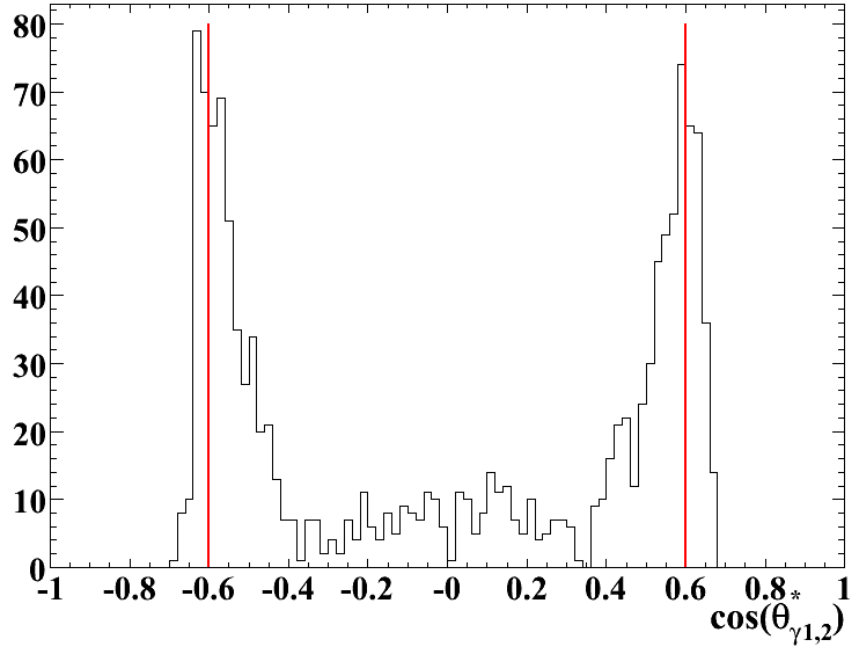


Figure 14: Distribution of reconstructed  $\cos\theta$  of the  $\gamma$  in CM system for  $p\bar{p} \rightarrow \pi^0\pi^0$  background.

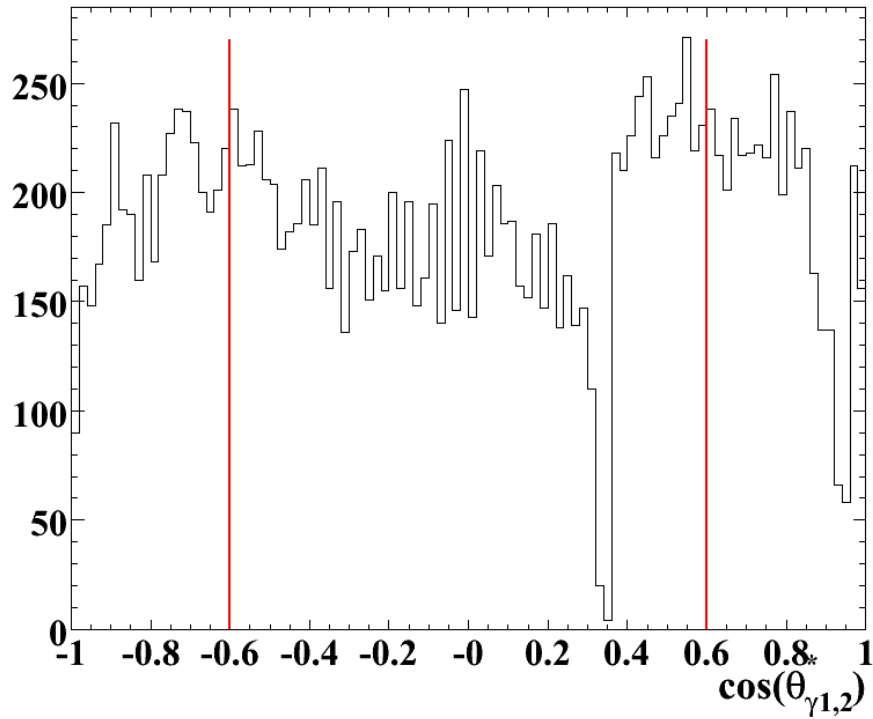


Figure 15: Distribution of reconstructed  $\cos\theta$  of the  $\gamma$  in CM system from  $h_c \rightarrow \eta_c\gamma$ .

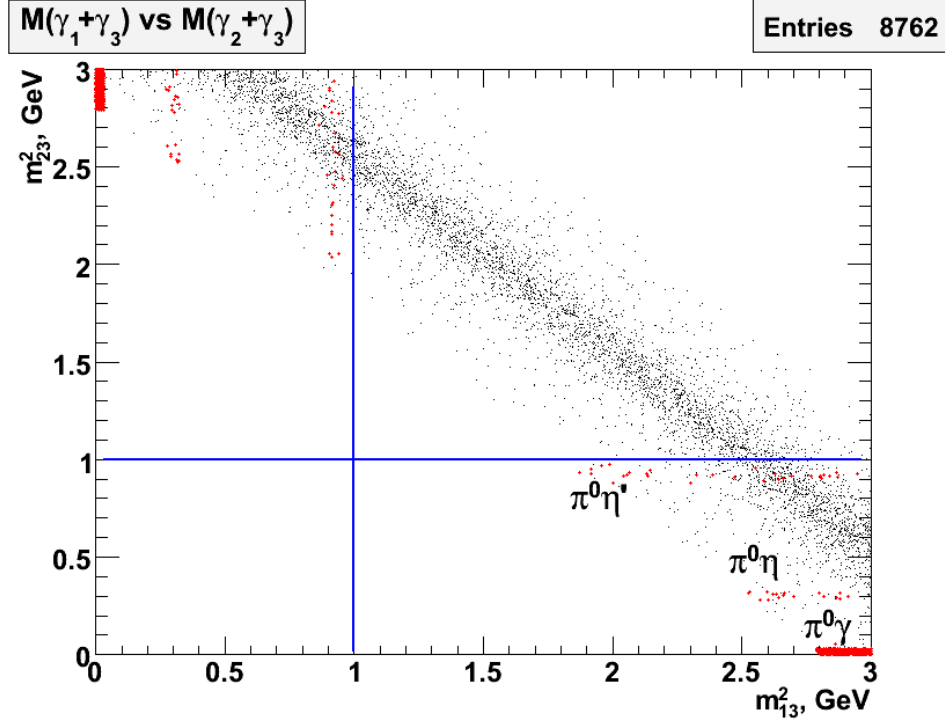


Figure 16: Dalitz plot for  $p\bar{p} \rightarrow \gamma\gamma\gamma$  events.

Cut	$h_c$	$\pi^0\gamma$	$\pi^0\pi^0$	$\pi^0\eta$	$\eta\eta$	$\pi^0\eta'$
preselection	0.70	0.43	0.14	$8.2 \cdot 10^{-2}$	$4.0 \cdot 10^{-2}$	$8.5 \cdot 10^{-2}$
$3 \gamma$	0.47	0.31	$1.3 \cdot 10^{-2}$	$7.5 \cdot 10^{-3}$	$2.7 \cdot 10^{-3}$	$8.7 \cdot 10^{-3}$
$CL > 10^{-4}$	0.44	0.30	$9.9 \cdot 10^{-3}$	$4.9 \cdot 10^{-3}$	$7.2 \cdot 10^{-4}$	$5.7 \cdot 10^{-3}$
$E_\gamma [0.4;0.6] \text{ GeV}$	0.43	0.12	$3.9 \cdot 10^{-3}$	$2.0 \cdot 10^{-3}$	$2.8 \cdot 10^{-4}$	$2.3 \cdot 10^{-3}$
$ \cos(\theta)  < 0.6$	0.22	$9.2 \cdot 10^{-2}$	$2.7 \cdot 10^{-3}$	$1.1 \cdot 10^{-3}$	$7.0 \cdot 10^{-5}$	$7.5 \cdot 10^{-4}$
$m_{12}^2, m_{23}^2 > 1.0 \text{ GeV}^2$	$8.1 \cdot 10^{-2}$	0	0	0	0	0

Table 4: Selection efficiencies for  $h_c \rightarrow 3\gamma$  and its background channels.

Channel	S/B ratio
$p\bar{p} \rightarrow \pi^0\pi^0$	$> 94$
$p\bar{p} \rightarrow \pi^0\gamma$	$> 164$
$p\bar{p} \rightarrow \pi^0\eta$	$> 88$
$p\bar{p} \rightarrow \eta\eta$	$> 87$
$p\bar{p} \rightarrow \pi^0\eta'$	$> 250$

Table 5: Signal to background ratio for  $h_c \rightarrow 3\gamma$  and different background channels.

with  $BR = 0.49$  [8].

## Background considerations

For the exclusive decay mode considered in this study:

$$\bar{p}p \rightarrow h_c \rightarrow \eta_c \gamma \rightarrow \phi \phi \gamma \rightarrow K^+ K^- K^+ K^- \gamma,$$

the following three reactions are considered as the main contributors to the background:

1.  $\bar{p}p \rightarrow K^+ K^- K^+ K^- \pi^0$ ,
2.  $\bar{p}p \rightarrow \phi K^+ K^- \pi^0$ ,
3.  $\bar{p}p \rightarrow \phi \phi \pi^0$ .

With one photon from the  $\pi^0$  decay undetected, these reactions have the same final state particles as the studied  $h_c$  decay.

Additional possible sources of background are:

4.  $\bar{p}p \rightarrow \Delta^{++}(1232)\bar{\Delta}^{--}(1232)\pi^0 \rightarrow p\pi^+\bar{p}\pi^-\pi^0$ ,
5.  $\bar{p}p \rightarrow K^+ K^- \pi^+ \pi^- \pi^0$ ,
6.  $\bar{p}p \rightarrow \pi^+ \pi^- \pi^+ \pi^- \pi^0$ .

The reaction #4 has been considered as one of the main sources of background in the Fermilab experiment E835 [1], which studied the same decay mode of  $h_c$ . This reaction has similar kinematics to the reaction of interest, i.e. 4 charged tracks in the forward direction. PANDA has significant advantages for discrimination of this source of background in comparison with E835, being equipped in magnetic analysis and PID tools. Nevertheless, an attempt was made to estimate explicitly the suppression factor for the reaction #5.

The last two reactions could contribute to background because of pion misidentification as kaons. In addition to PID such events can be effectively suppressed by the 4C-fit to beam energy-momentum. However, because of large cross-sections for these reactions, it seemed necessary to estimate the signal to background ratio for these channels in a detailed simulation.

Fig. 17 presents the distributions of  $\gamma$ 's in the laboratory energy for the signal and the background channel #3.

The energy range of  $\gamma$ 's from the  $h_c$  decay is [0.15; 2.0] GeV. The distribution for the background has different features. First, it is wider distributed extending beyond this energy range. Second, it has an increasing tendency towards zero energy. If we want to recover  $\pi^0$ 's to separate the signal from background, we should succeed to lower photon detection threshold as much as possible. Moreover, when one  $\gamma$  from the  $\pi^0$  decay has low

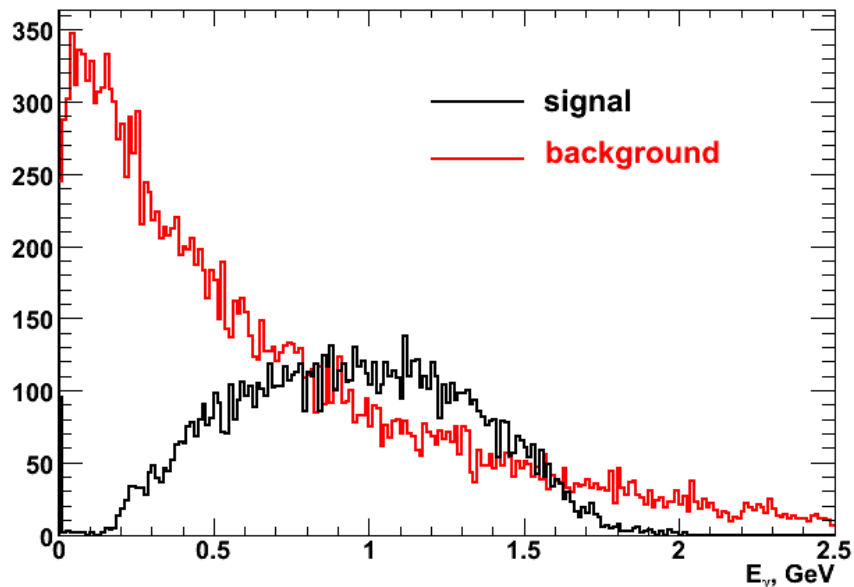


Figure 17: Energy distribution of the  $\gamma$  for the  $\bar{p}p \rightarrow h_c \rightarrow \eta_c \gamma$  and  $\bar{p}p \rightarrow \phi \phi \pi^0$  reactions.

energy, the other  $\gamma$  together with the charged hadrons has total momentum closer to the total momentum of the initial  $\bar{p}p$  system. Such events pass cuts on the fit probability of the 4C-fit and this increases the relative importance of the low energy threshold in order to apply a veto on  $\pi^0$ 's in an event and correspondingly to suppress background due to  $\pi^0$ 's.

There are no experimental measurements, to our best knowledge, of the cross-sections for the first three background reactions, which are supposed to be main contributors to background. The only way to estimate their cross-sections was found to use the DPM (Dual Parton Model) event generator [6].  $2 \cdot 10^7$  events were generated with DPM at the beam momentum  $p_z = 5.609 \text{ GeV}/c$ , which corresponds to the studied  $h_c$  resonance. The corresponding numbers of events are 115 and 12 for the first two background channels. No events for the  $\bar{p}p \rightarrow \phi \phi \pi^0$  reaction were observed. With the total  $\bar{p}p$  cross-section at this beam momentum of  $60 \text{ mb}$ , the cross-sections for the corresponding background channels are estimated at  $345 \text{ nb}$ ,  $60 \text{ nb}$  and below  $3 \text{ nb}$ , respectively. For the  $\bar{p}p \rightarrow \Delta^{++}(1232)\bar{\Delta}^{--}(1232)\pi^0$  and  $\bar{p}p \rightarrow \pi^+\pi^-\pi^+\pi^-\pi^0$  background channels the cross-section are known from the measurements at the  $\bar{p}$  beam momentum  $p = 5.7 \text{ GeV}/c$  [5] and [3]. The values are equal  $\sigma = 530 \mu\text{b}$  and  $\sigma = 750 \mu\text{b}$  respectively. For the purpose of estimation of signal to background ratio it was assumed that phase space engaged in the final state is uniformly populated. An estimate of the  $\bar{p}p \rightarrow K^+K^-\pi^+\pi^-\pi^0$  cross-section was done by extrapolating from lower energy according to the total inelastic cross-section. The result is  $\sigma = 30 \mu\text{b}$ .

Channel	N of events
$\bar{p}p \rightarrow h_c \rightarrow \phi\phi\gamma$	20 k
$\bar{p}p \rightarrow K^+K^-K^+K^-\pi^0$	6.2 M
$\bar{p}p \rightarrow \phi K^+K^-\pi^0$	200 k
$\bar{p}p \rightarrow \phi\phi\pi^0$	6.2 M
$\bar{p}p \rightarrow \Delta^{++}(1232)\bar{\Delta}^{--}(1232)\pi^0$	100 k
$\bar{p}p \rightarrow K^+K^-\pi^+\pi^-\pi^0$	5 M + 15 M
$\bar{p}p \rightarrow \pi^+\pi^-\pi^+\pi^-\pi^0$	1 M

Table 6: The numbers of analysed events for  $h_c$  decay and background reactions

## Analysed events and selection criteria

The numbers of analysed events are listed in Table 6. For the  $\bar{p}p \rightarrow K^+K^-\pi^+\pi^-\pi^0$  channel 15 millions out of 20 millions events were simulated with filter on invariant mass of the pair of two kaons. The events with  $m(K^+K^-)$  in the range [0.95;1.2] GeV were selected. The efficiency of the filter is 29.9 %, which gives effective number of simulated events  $\sim 55$  M.

The following selection criteria were applied:

1.  $\phi$  candidates were defined as  $K^+$ ,  $K^-$  pairs with invariant mass in the window [0.8 ; 1.2] GeV. Two  $\phi$  candidates in one event with invariant mass in the window [2.6 ; 3.2] GeV defined an  $\eta_c$  candidate which, combined with a neutral candidate, formed an  $h_c$  candidate.
2. A 4C-fit to beam energy-momentum was applied to the  $h_c$  candidate, which was stored to a root ntuple together with the updated information on its decay products.
3. The following additional cuts are performed at the ntuple level for background suppression:
  - (a) cut on the confidence level of the 4C-fit to beam energy-momentum,  $CL > 0.05$ ,
  - (b)  $\eta_c$  invariant mass within [2.9 ; 3.06] GeV,
  - (c)  $E_\gamma$  within [0.4 ; 0.6] GeV,
  - (d)  $\phi$  invariant mass within [0.99 ; 1.05] GeV,
  - (e) no  $\pi^0$  candidates in an event, i.e. no  $2\gamma$  invariant mass in the range [0.115 ; 0.15] GeV with two different low energy photon thresholds: 30 MeV and 10 MeV.

Fig. 18 presents the multiplicity distribution of reconstructed EMC clusters for the signal and one of the background channels. One may note that the mean number of neutral candidates exceeds one, the value expected for the signal, or two expected for the background from  $\pi^0$  decay. This is caused by hadronic split-offs, which make it impossible to select as the signal the events with only one cluster, because it leads to a significant

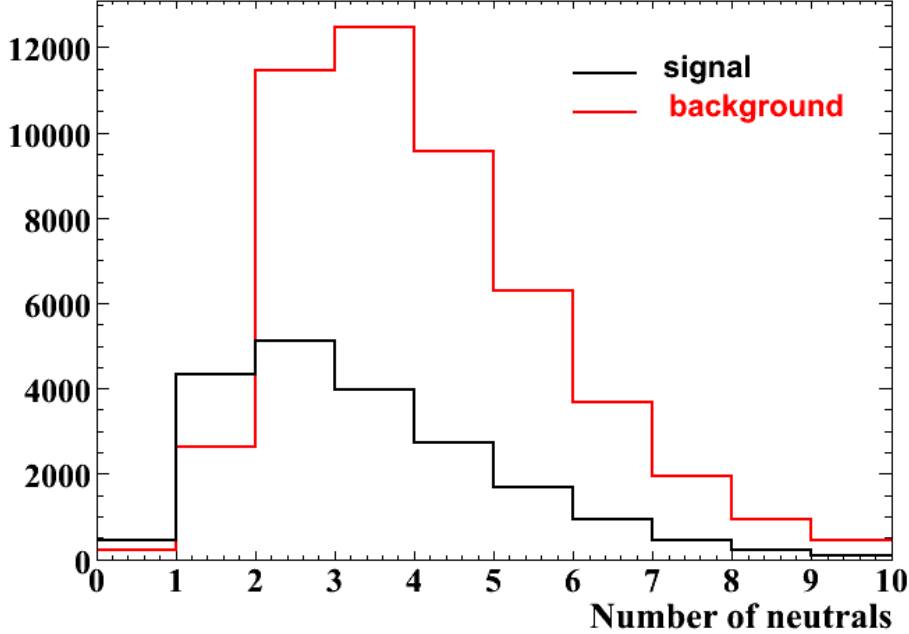


Figure 18: The number of reconstructed EMC clusters for the  $\bar{p}p \rightarrow h_c \rightarrow \eta_c \gamma$  and  $\bar{p}p \rightarrow \phi \pi^0$  reactions.

drop in efficiency. This observation emphasizes the importance of other selection criteria, in particular of the veto on  $\pi^0$  in an event. The effect of the latter requirement strongly depends on the assumed low energy photon threshold.

The distribution of  $K^+ - K^-$  pair invariant mass is presented in Fig. 19 for the signal and in Fig. 20 for the  $\bar{p}p \rightarrow K^+ K^- K^+ K^- \pi^0$  background. Windows on the mass of  $\phi$  are marked with vertical lines (in red).

## Signal to background ratio and the role of low-energy $\gamma$ -ray thresholds

The efficiencies of various cut selection criteria are listed in Table 7 for the signal and the first three of the considered background channels.

For the  $\bar{p}p \rightarrow K^+ K^- \pi^+ \pi^- \pi^0$  channel  $5 \cdot 10^6$  events have been analysed and only 35 of them passed the pre-selection criteria, which include loose mass windows, PID information and the requirement that the 4C-fit converges. No event passed the cut on CL in the 4C-fit. For  $\bar{p}p \rightarrow \Delta^{++}(1232)\bar{\Delta}^{--}(1232)\pi^0$  and  $\bar{p}p \rightarrow \pi^+ \pi^- \pi^+ \pi^- \pi^0$  no event has been found to pass pre-selection.

Assuming the  $h_c$  production cross-section of  $33nb$  at resonance, one obtains the signal to background ratios given in Table 8.

For the  $\bar{p}p \rightarrow \Delta^{++}(1232)\bar{\Delta}^{--}(1232)\pi^0$  and the  $\bar{p}p \rightarrow \pi^+ \pi^- \pi^+ \pi^- \pi^0$  channels, because of their large cross-sections, one needs around  $10^8$  events to make valid conclusions on background suppression at S/B levels above 1:1, which is not easy to fulfil because of

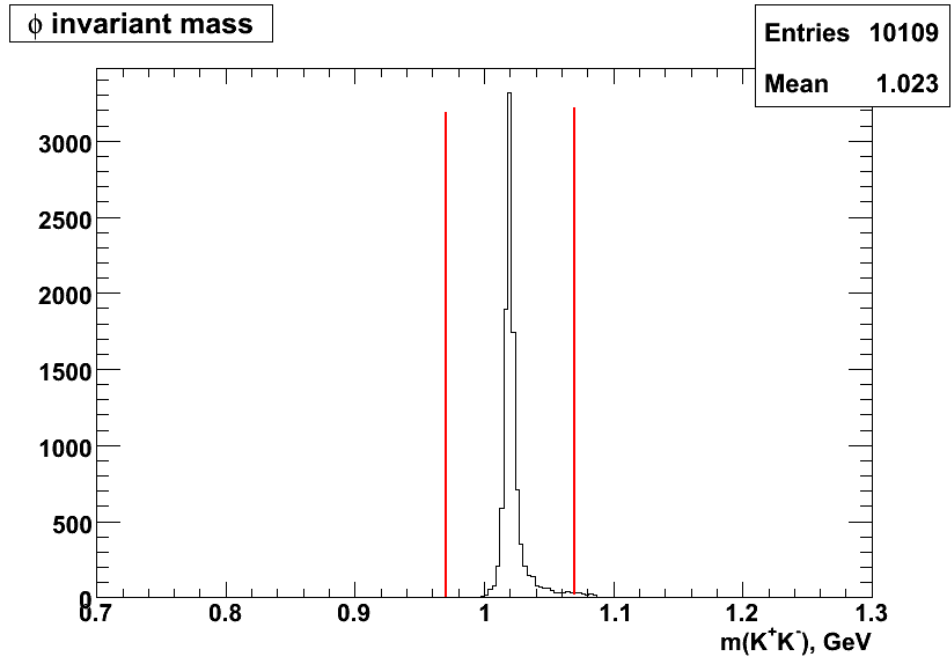


Figure 19: Invariant mass of  $K^+K^-$  with mass window on  $\phi$  for the  $h_c \rightarrow \phi\phi\gamma$ .

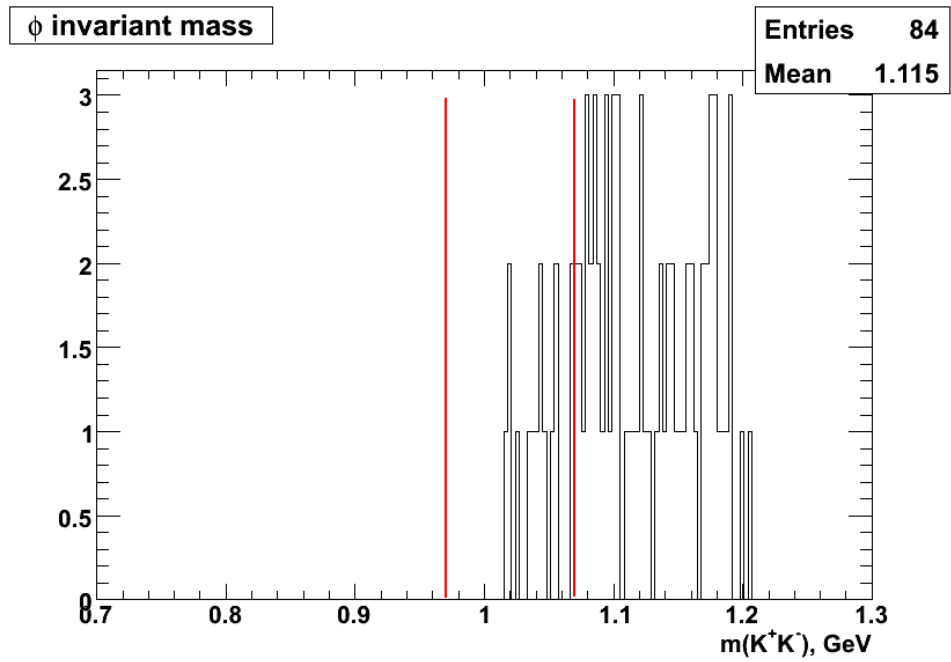


Figure 20: Invariant mass of  $K^+K^-$  with mass window on  $\phi$  for the  $p\bar{p} \rightarrow \phi\phi\pi^0$  background.

Selection criteria	signal	$4K\pi^0$	$\phi K^+K^-\pi^0$	$\phi\phi\pi^0$	$K^+K^-\pi^+\pi^-\pi^0$
pre-selection	0.51	$9.8 \cdot 10^{-3}$	$1.3 \cdot 10^{-2}$	$4.9 \cdot 10^{-2}$	$9.0 \cdot 10^{-6}$
$CL > 0.05$	0.36	$1.5 \cdot 10^{-3}$	$2.0 \cdot 10^{-3}$	$7.0 \cdot 10^{-3}$	$4.0 \cdot 10^{-8}$
$m(\eta_c), E_\gamma$	0.34	$4.1 \cdot 10^{-4}$	$5.2 \cdot 10^{-4}$	$1.8 \cdot 10^{-3}$	0
$m(\phi)$	0.31	$4.5 \cdot 10^{-6}$	$1.2 \cdot 10^{-4}$	$1.7 \cdot 10^{-3}$	0
$no \pi^0(30 MeV)$	0.26	$2.7 \cdot 10^{-6}$	$4.5 \cdot 10^{-5}$	$9.2 \cdot 10^{-4}$	0
$no \pi^0(10 MeV)$	0.24	$1.8 \cdot 10^{-6}$	$3.0 \cdot 10^{-5}$	$7.1 \cdot 10^{-4}$	0

Table 7: Efficiency of different event selection criteria.

channel	Signal/background ratio
$\bar{p}p \rightarrow K^+K^-K^+K^-\pi^0$	8
$\bar{p}p \rightarrow \phi K^+K^-\pi^0$	8
$\bar{p}p \rightarrow \phi\phi\pi^0$	> 10
$\bar{p}p \rightarrow K^+K^-\pi^+\pi^-\pi^0$	> 12

Table 8: Signal to background ratio for different  $h_c$  background channels.

the required excessive CPU time. The  $\bar{p}p \rightarrow K^+K^-\pi^+\pi^-\pi^0$  channel is more favorable from this point of view, having an order of magnitude smaller cross-section. However, it permits to study the influence of same factors, i.e. PID misidentification and power of the 4C-fit on background suppression. The latter channel requires only  $5 \cdot 10^6$  events to achieve valid conclusions on signal to background ratio (see Table 8).

For the  $\bar{p}p \rightarrow \phi\phi\pi^0$  background channel the reduction of low energy  $\gamma$ -ray threshold from 30 MeV to 10 MeV gives 20% improvement in the signal to background ratio, for the  $\bar{p}p \rightarrow \phi K^+K^-\pi^0$  the corresponding improvement is 40%.

With the final signal selection efficiency of 24% (see Table 7) and the assumed luminosity in high luminosity mode of  $L = 2 \cdot 10^{32} cm^{-2} s^{-1}$ , the expected signal event rate is 92 events/day. For the high resolution mode with  $L = 2 \cdot 10^{31} cm^{-2} s^{-1}$ , the expected signal event rate is 9 events/day, respectively.

## 4. Sensitivity to determination of the $h_c$ width

Finally, we want to investigate the sensitivity of PANDA to the determination of the  $h_c$  width. For this purpose we performed Monte Carlo simulations of energy scans around the resonance. Events were generated at 10 different energies around the  $h_c$  mass, each point corresponding to 5 days of measurements in high resolution mode.

The expected shape of measured resonance in  $\bar{p}p \rightarrow h_c \rightarrow \eta_c \gamma$  is the convolution of the Breit-Wigner resonance curve with the normalised beam energy distribution and an added

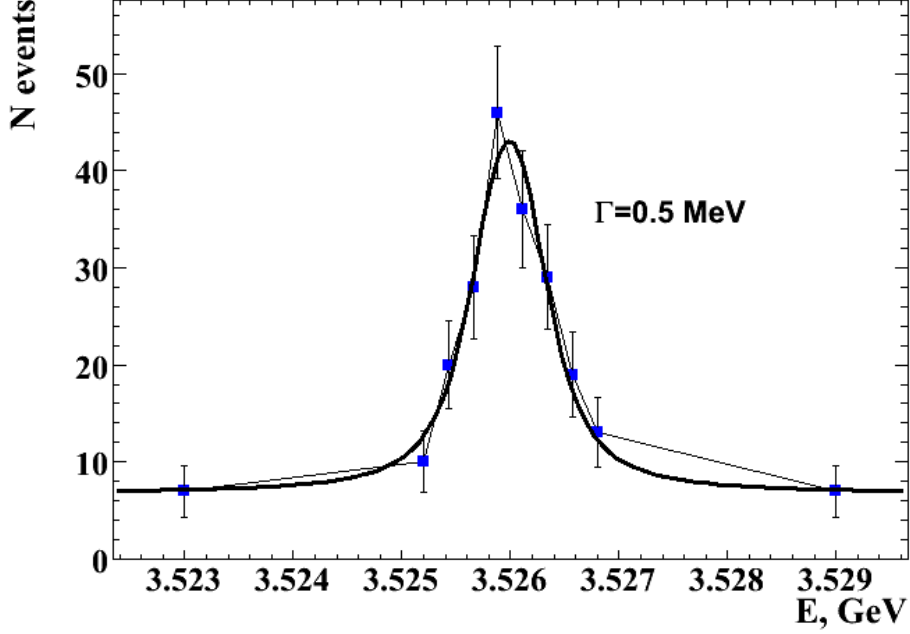


Figure 21: Fit of  $h_c$  resonance ( $\Gamma = 0.5$  MeV).

background term. The expected number of events at the  $i$ -th data point is:

$$\nu_i = [\varepsilon \times \int Ldt]_i \times [\sigma_{bkgd}(E) + \frac{\sigma_p \Gamma_R^2/4}{(2\pi)^{1/2} \sigma_i} \times \int \frac{e^{-(E-E')^2/2\sigma_i^2}}{(E' - M_R)^2 + \Gamma_R^2/4} dE'], \quad (3)$$

where  $\sigma_i$  is the beam energy resolution at the  $i$ -th data point,  $\Gamma_R$  and  $M_R$  the resonance width and mass,  $\sigma_p$  incorporates branching ratios for the formation and decay [see eq. (2)], the factor in square brackets in front of the r.h.s. of eq. (3) is the product of  $\varepsilon$ , an overall efficiency and acceptance factor and the integrated luminosity at the  $i$ -th point of measurements. To extract the resonance parameters the likelihood function,  $-\ln\mathcal{L}$ , is minimized assuming Poisson statistics, where:

$$\mathcal{L} = \prod_{j=1}^N \frac{\nu_j^{n_j} e^{-\nu_j}}{n_j!}. \quad (4)$$

For our simulation we assumed a signal to background ratio of 8:1 and we used the signal reconstruction efficiency of the  $h_c \rightarrow \eta_c \gamma \rightarrow \phi \phi \gamma$  channel. The simulated data were fitted to the expected signal shape with four free parameters:  $E_R$ ,  $\Gamma_R$ ,  $\sigma_{bkgd}$ ,  $\sigma_p$ . The background was assumed energy independent. The study has been repeated for three different  $\Gamma_R = 0.5, 0.75$  and  $1.0$  MeV. The results of the fit for  $0.5$  MeV and  $1.0$  MeV are presented in Fig. 21 and Fig. 22, respectively. The extracted  $\Gamma_R$ 's with errors are summarized in Table 9.

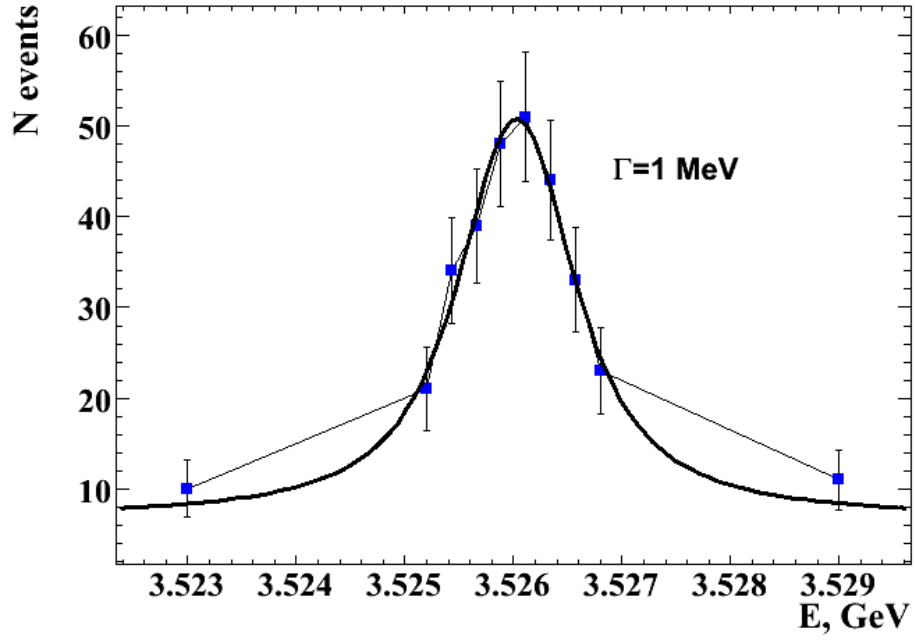


Figure 22: Fit of  $h_c$  resonance ( $\Gamma = 1$  MeV).

$\Gamma_{R,MC}$ , MeV	$\Gamma_{R,reco}$ , MeV	$\Delta\Gamma_R$ , MeV
1	0.92	0.24
0.75	0.72	0.18
0.5	0.52	0.14

Table 9: Reconstructed  $h_c$  width.

## References

- [1] M. Andreotti et al. Results of a search for the  $h_c(^1P_1)$  state of charmonium in the  $\eta_c\gamma$  and  $J/\psi\pi^0$  decay modes. *Phys. Rev.*, D72:032001, 2005.
- [2] M. Andreotti et al. Study of  $\bar{p}p \rightarrow$  two neutral pseudoscalar mesons at the  $\chi_{c0}(^1P_0)$  formation energy. *Phys. Rev.*, D72:112002, 2005.
- [3] R. Armenteros and B. French. Antinucleon-nucleon interactions. *High Energy Physics*, ed. by E.H.S. Burhop, IV:237, 1969.
- [4] T. A. Armstrong et al. Two-body neutral final states produced in antiproton - proton annihilations at  $2.911 \leq \sqrt{s} \leq 3.686$  GeV. *Phys. Rev.*, D56:2509–2531, 1997.
- [5] H. W. Atherton et al. The Reaction anti-p p  $\rightarrow$  anti-p p  $\pi^+\pi^-\pi^0$  at 5.7- GeV/c and a  $p\Omega^0$  (anti- $p\Omega^0$ ) Enhancement at 1.81 GeV. *Nuovo Cim.*, A30:505, 1975.
- [6] A. Capella et al. *Phys. Rept.*, 236:225, 1994.
- [7] J. L. Rosner et al. Observation of the  $h_c(^1P_1)$  state of charmonium. *Phys. Rev. Lett.*, 95:102003, 2005.
- [8] W.-M. Yao et al. Review of particle physics. *J. Phys. G: Nuclear and Particle Physics*, G33:1–1232, 2006.